Comparison Study of Industrial Robots for High-Speed Machining

Alexandr Klimchik, Alexandre Ambiehl, Sébastien Garnier, Benoît Furet, Anatol Pashkevich

Comparison study of industrial robots for high-speed machining

Alexandr Klimchik[1], Alexandre Ambiehl[2,3,4], Sebastien Garnier[2,3], Benoit Furet[2,3] and Anatol Pashkevich[2,5]

[1]Innopolis University, Universitetskaya St, 1, Innopolis, Tatarstan, 420500, Russia
[2]Institut de Recherches en Communications et en Cybernétique de Nantes, UMR CNRS 6597, 1 rue de la Noe, 44321 Nantes, France
[3]Université de Nantes, Chemin de la Censive du Tertre, 44300 Nantes, France
[4]Gébé 2 Productique, Parc Activite Vendée Sud Loire, 85600 Boufféré, France
[5]Ecole des Mines de Nantes, 4 rue Alfred-Kastler, 44307 Nantes, France
a.klimchik@innopolis.ru

Abstract. The paper presents methodology for comparison of industrial robots used for high-speed machining. Particular attention is paid to the robot accuracy in milling operation and evaluation robot capacity to perform the task with desired precision. In contrast to other works, the robot performance is evaluated using an industrial standard that is based on the distortion of the circular shape. The developed approach is applied to four industrial robots of KUKA family, which have been compared with respect to the machining precision.

Keywords: Robot-based machining, circularity index, industrial robot, stiffness model, compliance errors, robot comparison.

1 Introduction

High-speed machining is quite a new application of industrial robots. As follows form related study (Chen and Dong, 2013), the machining segment represents less than 5% of the total market of the industrial robots, but this share is continuously increasing. So, replacement of conventional CNC machines by more competitive industrial robots becomes more and more attractive. The main restraint here is rather limited knowledge of robotics by potential customers and lack of competence of the of robotic cell end-users. On the other side, the research labs have already confirmed that CNC machines replacement by robots gives essential benefits, which must be clarified for practicing engineers. For this reason, this paper proposes an industry oriented technique for evaluation of the robot capacities in machining, which can be used as the base for the related comparison study.

In contrast to conventional CNC machines, robots are able to process complex bulky 3D shapes and provide large and easily extendable workspace that can be modified by adding extra axes. Besides, the same workspace can be shared by several robots. However, the robot trajectory generation is much more complex task compared to the Cartesian machines since mapping from the actuator space to the operational space is highly non-linear. Another difficulty arises because of robot

redundancy with respect to the technological process. In fact, conventional machining process requires 5 dof only while most of industrial robots have 6 actuators. This redundancy can be used to optimize the tool path, to improve the trajectory smoothness (Zargarbashi et al., 2012a) or to minimize the impact of machining forces (Zargarbashi et al., 2012b, Vosniakos and Matsas, 2010).

Another difficulty of robot application in machining is related to non-negligible compliance of robotic manipulators. In some cases the end-effector deflections due to the influence of the cutting forces may overcome 10 mm (Matsuoka et al., 1999). To reduce them, robot manufactures pay particular attention to the manipulator stiffness and compensation of the compliance errors. To improve the manipulator rigidity, designers are obliged either to increase the link cross-sections or to use advanced composite materials. The first solution leads to increasing of moving masses and consequent reduction of dynamic properties. Utilization of composite materials essentially influences on the robot price and decreases its market competitiveness. Nevertheless, both ways improve the link stiffness only, while the major manipulator elasticity is often concentrated in the actuator gears (Dumas et al., 2012) and can be hardly improved in practice. Another method of the compliance error reduction is based on the mechanical gravity compensators. However, this solution does not allow compensating the impact of the machining forces. To overcome the problem of elastic deformations in the actuator gears, robot manufactures tends to use secondary encoders attached to the motor shaft (Devlieg, 2010) that allow to modify the actuator input in order to compensate the gear compliance. It is obvious that this approach also increases the robot price. According to our experience, the double encoders enable compensating about 65% of the compliance errors. The main reason for this is that the robot link deformations are outside of the double encoder observability. It is clear that for the high-speed milling, where the cutting forces are high enough to cause deflection of several millimeters, such level of error compensation is insufficient. In this case, it is reasonable to apply the off-line error compensation technique (Klimchik et al., 2013a, Chen et al., 2013) based on the modifying the reference trajectory used as the controller input. As follows from our previous research, this approach is very efficient. In particular, the off-line technique based on the simple (reduced) manipulator stiffness model allows user to compensate 85-90% of the end-effector deflections (Klimchik et al., 2012), while the complete stiffness model ensures the compensation level of about 95% (Klimchik et al., 2015). However, robot manufactures usually do not provide customers with the manipulator stiffness parameters, so they must carry out dedicated experimental study (Abele et al., 2007, Nubiola and Bonev, 2013). In this paper, the above mentioned problem will be also considered.

To advance robot application in machining, end-user should be provided with clear and efficient tool allowing to evaluate the final product quality expressed via the level of the end-effector deflections caused by the manipulator elasticity. It is evident that usual approach based on different performance measures extracted from the Cartesian stiffness matrix (Guo et al., 2015, Nagai and Liu, 2008) are not suitable here. For this reason, this paper proposes an industry oriented technique allowing to examine particular robot suitability for a give machining task and to compare several robot-based implementations.

2 Robot-based machining

Machining with robots is an intersection of two engineering fields: conventional machining and robotics. Machining sector usually prefers for these operations Cartesian CNC machines that provide end-users with high repeatability (2 μm) and good precision (5 μm). Traditionally, they are used for processing of metal parts from parallelepiped-like crude products with high material removal rate. Contemporary CNC machines possess quite large workspace allowing essentially increase an application area. Besides, their efficiency was also proved for processing of composite materials that are utilized more and more due to perfect mass-to-strength ratio. In addition to milling, finishing and trimming operations can be also performed by CNC machines. Nevertheless, in spite of numerous advantages, the CNC machines remain very expensive and their workspace is limited and cannot be extended, which is crucial for aeronautic and shipbuilding. This motivates users to find an alternative solution.

One of the promising ways to overcome the above mentioned difficulties is replacing the CNC machines by industrial robots, whose cost is competitive and workspace can be easily extended (by adding extra actuated axes). An example for such an application is presented in Fig. 1. Traditionally, the market of industrial robots is shared between handling, pick and place, assembling and welding. The processing (including machining), represents insignificant part of the market, less than 5%. According to PWC study (McCutcheon and Pethick, 2014) these shares will remain the same in the nearest future. Nevertheless, the share of robot-based machining is continuously growing. Large part of this market share corresponds to trimming that was traditionally a high-qualified manual work, but nowadays the robots become competitive here due to increasing of their accuracy. For machining, robots are attractive due to their large and extendable workspace and competitive price that makes them a cost-effective solution for machining of large dimension parts. However, the main obstacle for robots' utilization in machining is their relatively low accuracy (about 0.7 mm) and repeatability (about 0.2 mm) compared to the CNC machines. Nevertheless, there are a number of efficient solutions to reduce manipulator positioning errors that were discovered in research labs and progressively applied in industrial environment. The latter allows robots to compete with CNC machines in terms of accuracy, while providing essentially larger workspace.

Fig. 1. Example of machining process with robot

The problem of the machining process modeling has been known since pioneer work (Merchant, 1945), where Merchant used principle of minimum angle to develop an analytical 1D cutting force model based on chip thickness and material removal behavior. Latter, this model has been extended to the cases of 2D and 3D (Doi and Kato, 1955). The further advances in this area lead to mechanistic models (Koenigsberger and Sabberwal, 1961). These models explain the machining process as the function of the cutting tool geometry and process parameters (such as feed rate, spindle speed, etc). Further, the cutting force model was integration in the commercial software (Weck et al., 1994, Shirase and Altintaş, 1996). These models were able to predict deformation of the tool during machining and adapt cutting conditions (Wan et al., 2014, Araujo et al., 2015, Ali et al., 2013).

For the face milling application, the carbide insert tool cutting force model is the most advanced one allowing analyzing the path of each teeth and to predict corresponding force (Cheng et al., 1997). The geometry of technological process and corresponding cutting forces are given in Fig. 2. In the tool coordinate system, the instantaneous force $\mathbf{F}^i = [F_n{}^i, 0, F_f{}^i]^T$ is defined by the normal force F_n acting perpendicular to the tool face and the friction force F_f acting along the face. Here, the superscript "*i*" indicates the nature of the force, i.e. instantaneous. It should be noted that the friction force $F_f{}^i$ depends on normal force $F_n{}^i$ and friction coefficient k_f, i.e. $F_f{}^i = k_f \cdot F_n{}^i$. The normal force $F_n{}^i$ depends on the engagement angle φ, feed rate f_z and the cut depth a_p

$$F_n{}^i(\varphi) = K_n \cdot f_z \cdot a_p \cdot \sin\varphi \tag{1}$$

where K_n is a specific cutting coefficient, which depends on the material properties and the cutting tool.

The instantaneous force $\mathbf{F}^i$ is usually presented in the cylindrical coordinate system as $\mathbf{F}_0{}^i = [F_r{}^i, F_t{}^i, F_z{}^i]^T$, where F_r, F_t, F_z are the radial, tangential and axial forces, respectively. The correspondence between this forces are defined by the rotation matrix $\mathbf{R}(\kappa, \lambda_s, \gamma_0)$ that depends on the tool orientation, i.e. the entering angle κ, the helix angle λ_s and the cutting angle γ_0

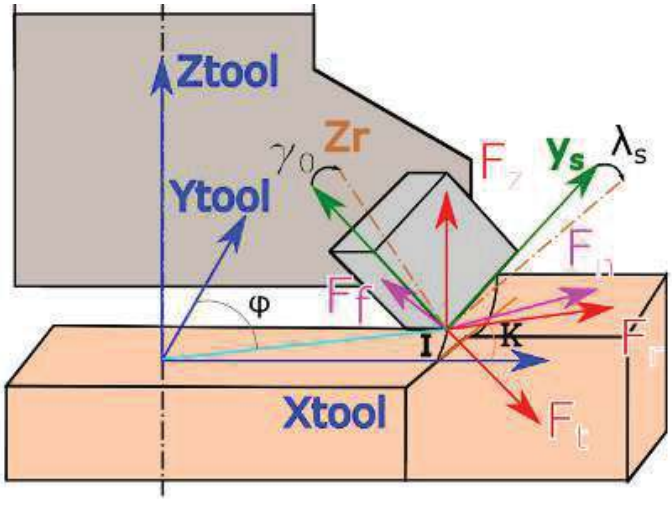

Fig. 2. Cutting force in the machining process

$$\mathbf{F}_0^{\,i} = \mathbf{R}\left(\kappa, \lambda_s, \gamma_0\right) \cdot \mathbf{F}^i \tag{2}$$

Using cylindrical coordinate system, it is possible to project the cutting force to the workpiece frame,

$$\mathbf{F}_C^{\,i} = \mathbf{R}_z\left(\varphi\right) \cdot \mathbf{F}_0^{\,i} \tag{3}$$

where $\mathbf{F}_C$ is the cutting force in the Cartesian space, $\mathbf{R}_z$ is the homogeneous rotation matrix and φ is the engagement angle. The cutting force varies with the engagement angle φ, so in practice the force usually is evaluated for the complete tool revolution and can be computed as

$$F_n = \int_{\varphi_S}^{\varphi_E} F_n^{\,i} d\varphi \tag{4}$$

where φ_S and φ_E are the start and end angles for the tool engagement. The engagement angles φ_S, φ_E are defined by the technological task and cutting tool diameter.

Similarly, the cutting force in the Cartesian coordinate system can be computed as

$$\mathbf{F}_C = \int_{\varphi_S}^{\varphi_E} \mathbf{R}_z\left(\varphi\right) \cdot \mathbf{R}\left(\kappa, \lambda_s, \gamma_0\right) \cdot \mathbf{F}_0^{\,i}\, d\varphi \tag{5}$$

Taking into account that $\mathbf{F} = F_n \cdot \mathbf{C}$ with $\mathbf{C} = [1,\, 0,\, k_f\,]^T$, one can rewrite the cutting force expression in the following form

$$\mathbf{F}_C = \int_{\varphi_S}^{\varphi_E} F_n\left(\varphi\right) \cdot \mathbf{R}_z\left(\varphi\right)\, d\varphi \cdot \mathbf{R}\left(\kappa, \lambda_s, \gamma_0\right) \cdot \mathbf{C} \tag{6}$$

The latter can be used to compute the cutting force that is applied to the robot end-effector.

Once the cutting force is known, it is possible to estimate the torques generated by the cutting force at the tool reference frame $\mathbf{M} = \mathbf{r} \times \mathbf{F}_0$. Here, $\mathbf{r} = [r\cos\varphi,\, r\sin\varphi,\, 0]^T$, r is the tool radius. In this case, the torque with respect to the tool contact point can be computed as

$$\mathbf{M} = F_n \cdot (\mathbf{r}\times) \cdot \mathbf{R}\left(\kappa, \lambda_s, \gamma_0\right) \cdot \mathbf{C} \tag{7}$$

where $(\mathbf{r}\times)$ is the skew-symmetric matrix based on the vector $\mathbf{r}$. Further, this torque can be transferred to the robot end-effector taking into account the tool and spindle geometry.

3 Compliance errors and their estimation

3.1 Manipulator positioning errors under the loading

In robotics, manipulator stiffness is usually described by the Cartesian stiffness matrix $\mathbf{K}_C$ that allows user to compute the end-effector deflections $\Delta\mathbf{t}$ as

$$\Delta\mathbf{t} = \mathbf{K}_C^{-1} \cdot \mathbf{F} \tag{8}$$

for given external force $\mathbf{F}$. Using the VJM-based technique (Pashkevich et al., 2011), the stiffness model of a typical industrial robot is presented as a serial chain containing rigid links separated by actuators and virtual springs (Kövecses and Angeles, 2007) as shown in Fig. 3.

To compute the Cartesian stiffness matrix, it is necessary to consider simultaneously the extended geometric model $\mathbf{t} = \mathbf{g}(\mathbf{q}, \boldsymbol{\theta})$ and static equilibrium equation $\mathbf{J}_\theta^T \cdot \mathbf{F} = \mathbf{K}_\theta \cdot \boldsymbol{\theta}$. The first of them allows computing the end-effector location $\mathbf{t}$ for given actuator coordinates $\mathbf{q}$ and virtual joint deflections $\boldsymbol{\theta}$ caused by the loading $\mathbf{F}$. The static equilibrium equation allows finding relation between the external force and the deflections of the virtual joints. It includes the matrix $\mathbf{K}_\theta$ describing the virtual joint elasticities and the Jacobian of the extended geometric model $\mathbf{J}_\theta = \partial\mathbf{g}(\mathbf{q}, \boldsymbol{\theta}) / \partial\boldsymbol{\theta}$. Simultaneous solution of the above mentioned equations leads to the following expression for the desired Cartesian stiffness matrix

$$\mathbf{K}_C = \left(\mathbf{J}_\theta \cdot \mathbf{K}_\theta^{-1} \cdot \mathbf{J}_\theta^T\right)^{-1} \tag{9}$$

In more general case, when the external loading $\mathbf{F}$ is rather high, the Cartesian stiffness matrix also depends on the Hessian $\mathbf{H}_{\theta\theta}$ (Klimchik et al., 2014a). So, the above equation is replaced by.

$$\mathbf{K}_C = \left(\mathbf{J}_\theta \cdot (\mathbf{K}_\theta - \mathbf{H}_{\theta\theta})^{-1} \cdot \mathbf{J}_\theta^T\right)^{-1} \tag{10}$$

where $\mathbf{H}_{\theta\theta} = \partial^2(\mathbf{g}(\mathbf{q}, \boldsymbol{\theta}) \cdot \mathbf{F}) / \partial\boldsymbol{\theta}^2$ describes modification of manipulator elasticity due to applied loading.

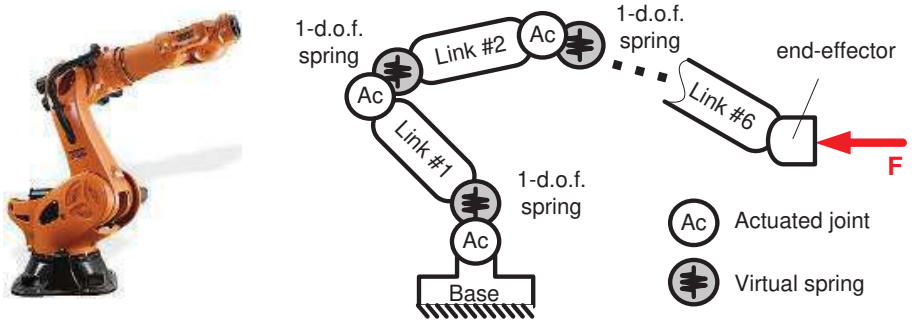

(a) Typical industrial robot (b) VJM model of serial robot

Fig. 3. Typical industrial robot and its VJM-based stiffness model.

The above expressions for the Cartesian stiffness matrix were derived assuming that joint stiffness matrix $\mathbf{K}_\theta$ is constant. However, if the manipulator includes the gravity compensators, the equivalent joint stiffness coefficients become configuration dependent and the joint stiffness matrix is presented as a sum

$$\mathbf{K}_\theta = \mathbf{K}_\theta^0 + \mathbf{K}_\theta^{GC}(\mathbf{q}) \tag{11}$$

where the first term $\mathbf{K}_\theta^0$ is constant and corresponds to the manipulator without compensator; and the second term $\mathbf{K}_\theta^{GC}(\mathbf{q})$ depends on the manipulator configuration and describes equivalent elasticity of the gravity compensator with respect to the virtual joints. More details concerning computing of these matrices are given in our previous work (Klimchik et al., 2013b).

3.2 Evaluation of machining accuracy using circularity

In the industrial practice, there exist different norms to evaluate the final product quality. For example, ISO 12780 and 12781 define the path straightness, the surface flatness and the path roundness that in some cases is also called as the *circularity*. From our experience, the circularity index is the best one for evaluating the machining process quality, since for linear trajectories the force magnitude/direction are constant and their impact can be easily compensated in the control program (Feng et al., 2015). In contrast, for the circular path the cutting force direction varies and may lead to irregular path distortion that can be hardly compensated. For this reason, the circularity index will be used to evaluate the capacity of industrial robot to perform the machining task.

According to ISO 12181, the circularity evaluation includes two steps: obtaining a reference circle and estimation of the path deviations with respect to this circle. There are four methods to define the reference circle: Minimum Circumscribed Circle (MCC), Maximum Inscribed Circle (MIC), Minimum Zone Circles (MZC) and Least Squares Circle (LSC). They are illustrated by Fig. 4. For all of them, the circularity evaluates the distance between two circles in accordance with the equation

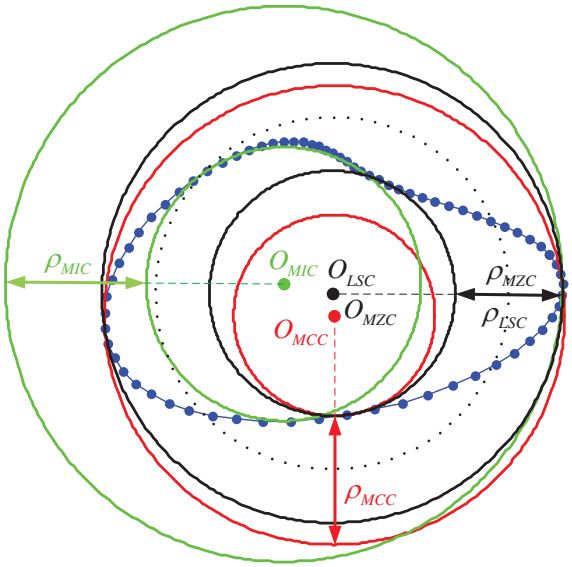

Fig. 4. Circularity evaluation using different industrial norms.

$$\rho = r_{\max} - r_{\min} \tag{12}$$

where $r_{\max}$ and $r_{\min}$ are the radii of the circumscribed and inscribed circles, respectively. The principal difference is related to the circle centers that are computed using different methods. For example, for MIC the center point is computed for the maximum inscribed circle and it is also used for the minimum circumscribed one. In the MCC method, the center is computed for the minimum circumscribed circle and the inscribed circle is build using the same center point. In the case of LSC, the inscribed and circumscribed circles are found for the center point obtained for the least square circle. In contrast, the MZC method uses a center point for which the distance between the inscribed and circumscribed circles is minimal. In practice, MIC and MCC methods are rarely used if the tool path is essentially distorted and corresponding center points are essentially different (Fig. 4). In the latter case, it is preferable to use either MZC or LSC index. Since there is no considerable difference between MZC or LSC, practicing engineers prefer LSC to evaluate the trajectory circularity.

In the frame of the LSC method, the circle center is obtained as a solution of the following optimization problem

$$\sum_{i=1}^{n} (\sqrt{(x_i - x_0)^2 - (y_i - y_0)^2} - r)^2 \to \min_{x_0, y_0, r} \tag{13}$$

where (x_i, y_i) are the measured tool path coordinates, (x_0, y_0) is the circle center and r is its radius. This optimization problem is highly non-linear and cannot be solved analytically. For this reason, a Newton–Raphson method is used.

Using the LSC center point, the circularity is computed in straightforward way in accordance with (12), where

$$r_{\max} = \max(|\mathbf{p}_i - \mathbf{O}_{LS}|, i = \overline{1,n}); \qquad r_{\min} = \min(|\mathbf{p}_i - \mathbf{O}_{LS}|, i = \overline{1,n}) \tag{14}$$

Here $\mathbf{p}_i = (x_i, y_i)^T$ is measured tool path points and $\mathbf{O}_{LS} = (x_0, y_0)^T$ is the center of corresponding LS circle.

Assuming that all geometric and elastostatic parameters of the manipulator are known, the resulting tool path for the desired circular trajectory can be computed and evaluated the above presented index. For the set of machining tasks considered in this paper, a benchmark trajectory is a circle of radius 100 mm. For each task and for each path point, there were computed the cutting wrenches $\mathbf{W} = [\mathbf{F}_C{}^T, \mathbf{M}^T]^T$ which include both the force and the torque components. It is worth mentioning, that the wrench magnitude is constant here, while its direction varies along the path depending on the rotation angle φ. Using this data, the resulting tool path can be computed in the following way

$$\mathbf{p}_i = \mathbf{p}_0 + \mathbf{R}\,\mathbf{r} + \mathbf{J}_\theta^{(\mathrm{p})} \cdot \mathbf{K}_\theta^{-1} \; \mathbf{J}_\theta^{(\mathrm{p})\mathrm{T}} \mathbf{R}\,\mathbf{F}_C + \mathbf{J}_\theta^{(\mathrm{p})} \cdot \mathbf{K}_\theta^{-1} \cdot \mathbf{J}_\theta^{(\varphi)\mathrm{T}} \mathbf{R}\,\mathbf{M} \tag{15}$$

where $\mathbf{p}_0$ is the center of the reference circle, r is its radius, $\mathbf{r}$ defines the radius vector of the circle for $\varphi = 0$, the matrix $\mathbf{R}(\varphi_i)$ takes into account rotation of the target point by the angle φ_i, the superscripts (p) and (φ) indicate the position and orientation part of the Jacobian matrix presented as $\mathbf{J}_\theta = [\mathbf{J}_\theta^{(p)\mathrm{T}}, \mathbf{J}_\theta^{(\varphi)\mathrm{T}}]^T$. It should be stressed that dynamics also affects the circularity; however, its influence is much lower comparing to the compliance errors caused by cutting forces.

Based on this approach, it is possible to evaluate robot accuracy with respect to the circularity index for the entire workspace and to determine the region in which machining accuracy is the best (from the circularity point of view).

4 Experimental result

The technique developed in this paper has been applied to the comparison study of four industrial robots of Kuka family. There were compared with respect to the circular machining task of 100 mm radius that was placed in different workspace points. Some details concerning the examined robots and their principal parameters are given in Table 1. These robots have similar kinematics and provide comparable repeatability/accuracy without loading. However, their payload capacities and workspace size are different. Elastostatic parameters of the examined robots have been identified using dedicated experimental study using methodology developed in our previous works (Klimchik et al., 2013b, Klimchik et al., 2014b). Corresponding results are presented in Table 2.

In the experimental study, it was used the cutting tool of the radius $R = 5mm$ with three teeth ($z = 3$). Its machining parameters are the following: $\kappa = 90°$, $\gamma_0 = 7°$, $\lambda_s = 45°$, $f_z = 0.08\ mm/rev$, $a_p = 5\ mm$, $K_n = 750\,N/\mathrm{mm}^2$. It is assumed that cutting tool is completely engaged ($\varphi = 180°$) along the trajectory. This corresponds the cutting force $\mathbf{F}_C = [-440N, -1370N, -635N]$ and cutting torque $\mathbf{M} = [0Nm, 3Nm, 10.5Nm]$. These vectors are rotating while the tool is moving along the circular trajectory.

Table 1. Principal characteristics of examined robots.

Robot	Repeatability	Workspace volume	Working radius,	Maximum payload
KR 100 HA	0.05 mm	46 m^3	2.6 m	100 kg
KR270	0.06 mm	55 m^3	2.7 m	270 kg
KR360	0.08 mm	118 m^3	3.3 m	360 kg
KR500	0.08 mm	68 m^3	2.8 m	500 kg

Table 2. Stiffness parameters of examined robots.

Robot	Equivalent joint compliances, μm/N					
	k_1	k_2	k_3	k_4	k_5	k_6
KR100 HA	1.92	0.34	0.56	3.31	3.83	5.42
KR270	0.54	0.29	0.42	2.79	3.48	2.07
KR360	0.86	0.17	0.25	2.17	1.47	2.96
KR500	0.47	0.14	0.19	0.72	0.95	1.44

In our study it was assumed that the reference circular trajectory was located in the plane of joint q_2 and q_3 movements (XOZ if q_1=0), which is the most critical one for all articulated robots in machining application. For these conditions, the circularity maps have been computed for all examined manipulators. Relevant results are presented in Figures 5-8. In addition, these figures contain the optimal regions for locating the machining tasks of size 100×100, 200×200 and 500×500 mm. Summary of circularity indices for different machining task is given in Table 3. It should be stressed that in the case of machining task different from the considered one, the results should be scaled according to cutting force magnitude.

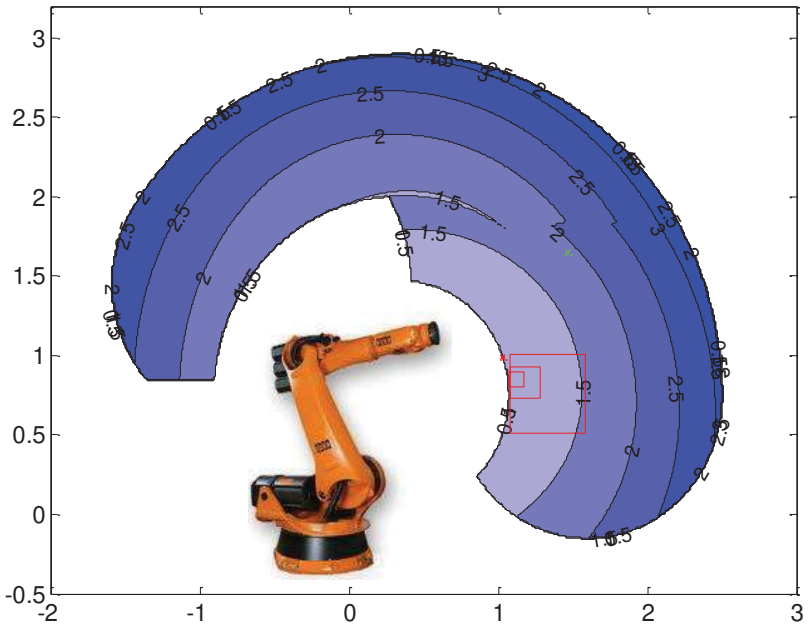

Fig. 5. Circularity maps for robot KR 100 HA.

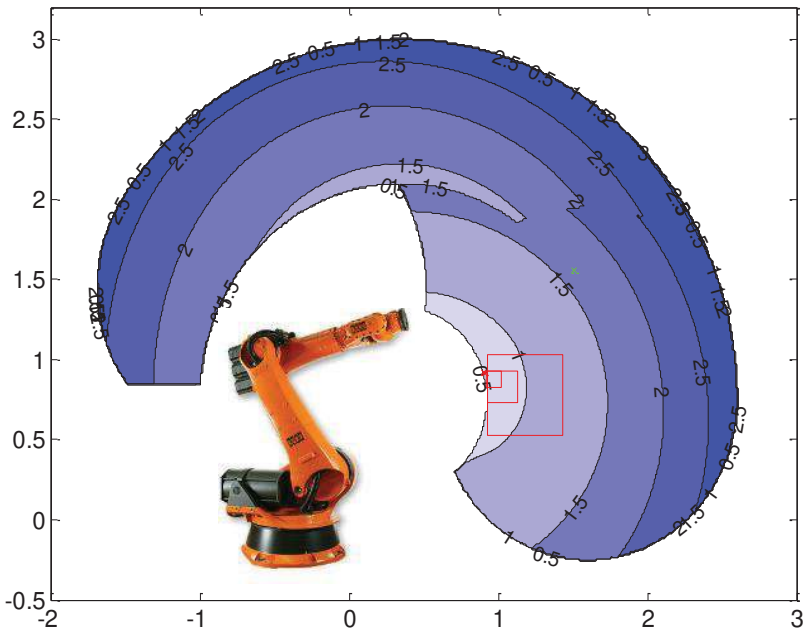

Fig. 6. Circularity maps for robot KR 270.

Table 3. Circularity indices for examined robots, mm.

Robot	min	max	Middle
KR 100 HA	1.03	3.36	1.91
KR270	0.84	3.13	1.64
KR360	1.02	2.81	1.80
KR500	0.41	1.42	0.76

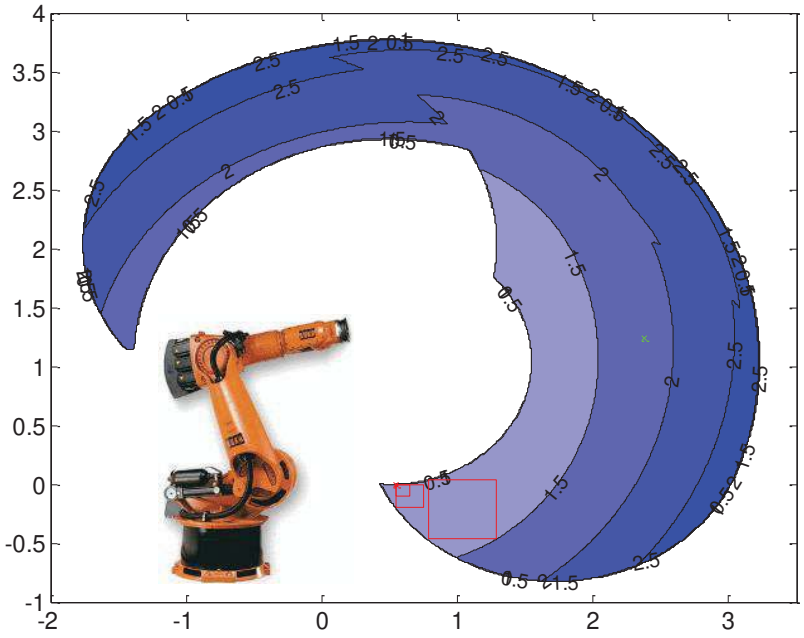

Fig. 7. Circularity maps for robot KR 360.

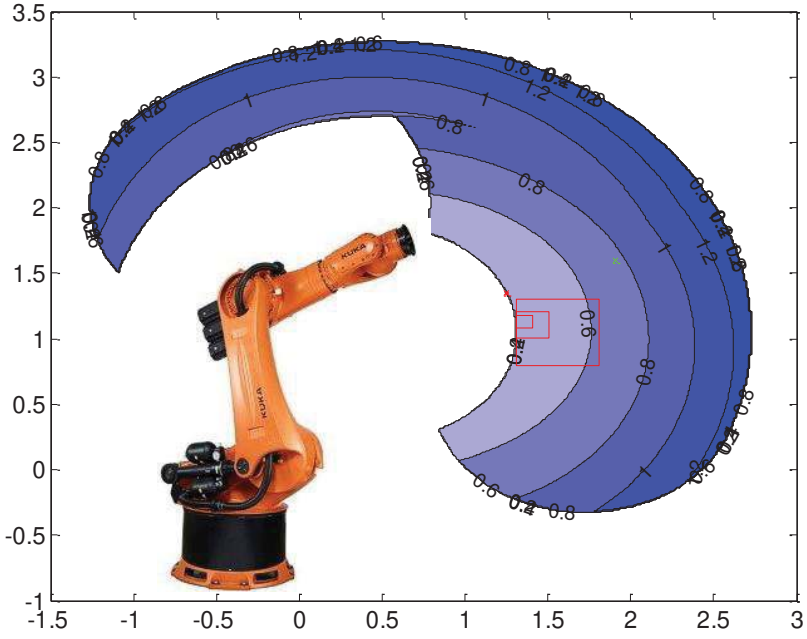

Fig. 8. Circularity maps for robot KR 500.

Table 4. Suitability of examined robots for different machining tasks (without compensation).

Circularity	Force magnitude			
	500N	1000N	2000N	3000N
0.2 mm	KR 500			
0.5 mm	KR100 KR 270 KR 360 KR 500	KR 270 KR 500	KR 500	
1.0 mm	KR 100 KR 270 KR 360 KR 500	KR100 KR 270 KR 360 KR 500	KR 270 KR 360 KR 500	KR 500
1.5 mm	KR100 KR 270 KR 360 KR 500	KR 100 KR 270 KR 360 KR 500	KR 270 KR 360 KR 500	KR 500
2.0 mm	KR 100 KR 270 KR 360 KR 500	KR 100 KR 270 KR 360 KR 500	KR 270 KR 360 KR 500	KR 360 KR 500

As follows from the presented results, robot Kuka KR500 ensures the best performance for the considered technological task. This advantage is achieved due to less complaint actuators, which obviously affect the robot price. In general, all examined robots ensure circularity level about 3 mm within entire workspace (without compensation). So, if this accuracy is sufficient, the robot can be chosen taking into account the workspace and payload properties. It should be stressed that robot KR100 cannot be used for machining of hard materials because of the payload limitation. However, because of its lower price comparing to other examined robots, it is competitive for machining if the cutting force magnitude is less than 1kN and the desired circularity is about 1 mm. On the other hand, robot KR360 is competitive for large-dimensional tasks only and for milling with forces higher than 2.5kN. Otherwise, KR270 is preferable that may ensure better performance within its workspace. The obtained results are also summarized in Table 4 that presents robots suitable for machining with desired accuracy (in terms of the circularity) for different force magnitudes. The latter allows practicing engineers to justify robot selection for given machining task.

5 Conclusions

The paper presents an industry oriented technique for evaluation of robot capacity to perform machining operations. It proposes methodology for evaluation of the circularity widely used in industrial practice. Obtained theoretical results have been applied to the experimental study that provides comparison analysis of four industrial robots with respect to their accuracy in machining. In future, this methodology will be applied to a wider set of industrial robots, technological tools and materials.

6 Acknowledgments

The work presented in this paper was partially funded by the project FEDER ROBOTEX № 38444, France.

References

Abele, E., Weigold, M. & Rothenbücher, S. (2007) Modeling and Identification of an Industrial Robot for Machining Applications. *CIRP Annals - Manufacturing Technology,* **56** (1)**,** 387-390.

Ali, M. H., Khidhir, B. A., Ansari, M. N. M. & Mohamed, B. (2013) FEM to predict the effect of feed rate on surface roughness with cutting force during face milling of titanium alloy. *HBRC Journal,* **9** (3)**,** 263-269.

Araujo, A. C., Mello, G. M. & Cardoso, F. G. (2015) Thread milling as a manufacturing process for API threaded connection: Geometrical and cutting force analysis. *Journal of Manufacturing Processes,* **18,** 75-83.

Chen, Y. & Dong, F. (2013) Robot machining: recent development and future research issues. *The International Journal of Advanced Manufacturing Technology,* **66** (9-12)**,** 1489-1497.

Chen, Y., Gao, J., Deng, H., Zheng, D., Chen, X. & Kelly, R. (2013) Spatial statistical analysis and compensation of machining errors for complex surfaces. *Precision Engineering,* **37** (1)**,** 203-212.

Cheng, P. J., Tsay, J. T. & Lin, S. C. (1997) A study on instantaneous cutting force coefficients in face milling. *International Journal of Machine Tools and Manufacture,* **37** (10)**,** 1393-1408.

Devlieg, R. (2010) Expanding the use of robotics in airframe assembly via accurate robot technology. SAE Technical Paper.

Doi, S. & Kato, S. (1955) Chatter vibration of lathe tools. ASME.

Dumas, C., Caro, S., Cherif, M., Garnier, S. & Furet, B. (2012) Joint stiffness identification of industrial serial robots. *Robotica,* **30** (04)**,** 649-659.

Feng, W. L., Yao, X. D., Azamat, A. & Yang, J. G. (2015) Straightness error compensation for large CNC gantry type milling centers based on B-spline curves modeling. *International Journal of Machine Tools and Manufacture,* **88,** 165-174.

Guo, Y., Dong, H. & Ke, Y. (2015) Stiffness-oriented posture optimization in robotic machining applications. *Robotics and Computer-Integrated Manufacturing,* **35,** 69-76.

Klimchik, A., Chablat, D. & Pashkevich, A. (2014a) Stiffness modeling for perfect and non-perfect parallel manipulators under internal and external loadings. *Mechanism and machine theory,* **79,** 1-28.

Klimchik, A., Furet, B., Caro, S. & Pashkevich, A. (2015) Identification of the manipulator stiffness model parameters in industrial environment. *Mechanism and machine theory,* **90,** 1-22.

Klimchik, A., Pashkevich, A., Chablat, D. & Hovland, G. (2013a) Compliance error compensation technique for parallel robots composed of non-perfect serial chains. *Robotics and Computer-Integrated Manufacturing,* **29** (2)**,** 385-393.

Klimchik, A., Pashkevich, A., Wu, Y., Caro, S. & Furet, B. (2012) Design of calibration experiments for identification of manipulator elastostatic parameters. *Applied Mechanics and Materials,* **162,** 161-170.

Klimchik, A., Wu, Y., Caro, S., Furet, B. & Pashkevich, A. (2014b) Geometric and elastostatic calibration of robotic manipulator using partial pose measurements. *Advanced Robotics,* **28** (21)**,** 1419-1429.

Klimchik, A., Wu, Y., Dumas, C., Caro, S., Furet, B. & Pashkevich, A. (2013b) Identification of geometrical and elastostatic parameters of heavy industrial robots. *IEEE International Conference on Robotics and Automation (ICRA)*

Koenigsberger, F. & Sabberwal, A. J. P. (1961) An investigation into the cutting force pulsations during milling operations. *International Journal of Machine Tool Design and Research,* **1** (1–2)**,** 15-33.

Kövecses, J. & Angeles, J. (2007) The stiffness matrix in elastically articulated rigid-body systems. *Multibody System Dynamics,* **18** (2)**,** 169-184.

Matsuoka, S.-i., Shimizu, K., Yamazaki, N. & Oki, Y. (1999) High-speed end milling of an articulated robot and its characteristics. *Journal of Materials Processing Technology,* **95** (1–3)**,** 83-89.

McCutcheon, R. & Pethick, R. (2014) The new hire: How a new generation of robots is transforming manufacturing. Price waterhouse Coopers

Merchant, M. E. (1945) Mechanics of the metal cutting process. I. Orthogonal cutting and a type 2 chip. *Journal of applied physics,* **16** (5)**,** 267-275.

Nagai, K. & Liu, Z. (2008) A systematic approach to stiffness analysis of parallel mechanisms. *Robotics and Automation, 2008. ICRA 2008. IEEE International Conference on.* IEEE.

Nubiola, A. & Bonev, I. A. (2013) Absolute calibration of an ABB IRB 1600 robot using a laser tracker. *Robotics and Computer-Integrated Manufacturing,* **29** (1)**,** 236-245.

Pashkevich, A., Klimchik, A. & Chablat, D. (2011) Enhanced stiffness modeling of manipulators with passive joints. *Mechanism and machine theory,* **46** (5)**,** 662-679.

Shirase, K. & Altintaş, Y. (1996) Cutting force and dimensional surface error generation in peripheral milling with variable pitch helical end mills. *International Journal of Machine Tools and Manufacture,* **36** (5)**,** 567-584.

Vosniakos, G.-C. & Matsas, E. (2010) Improving feasibility of robotic milling through robot placement optimisation. *Robotics and Computer-Integrated Manufacturing,* **26** (5)**,** 517-525.

Wan, M., Pan, W.-J., Zhang, W.-H., Ma, Y.-C. & Yang, Y. (2014) A unified instantaneous cutting force model for flat end mills with variable geometries. *Journal of Materials Processing Technology,* **214** (3)**,** 641-650.

Weck, M., Altintas, Y. & Beer, C. (1994) CAD assisted chatter-free NC tool path generation in milling. *International Journal of Machine Tools and Manufacture,* **34** (6)**,** 879-891.

Zargarbashi, S. H. H., Khan, W. & Angeles, J. (2012a) The Jacobian condition number as a dexterity index in 6R machining robots. *Robotics and Computer-Integrated Manufacturing,* **28** (6)**,** 694-699.

Zargarbashi, S. H. H., Khan, W. & Angeles, J. (2012b) Posture optimization in robot-assisted machining operations. *Mechanism and machine theory,* **51,** 74-86.